January 2018

Mechanisms Of Decreased Brainstem Arousal In Limbic Seizures: In Vivo Whole-Cell Recordings

John Paul Andrews

Mechanisms of decreased brainstem arousal in limbic seizures: *in vivo* whole-cell recordings

A Thesis Submitted to the
Yale University School of Medicine
in Partial Fulfillment of the Requirements for the
Degree of Doctor of Medicine

by

John Paul Andrews

2018

Abstract

Seizures are commonly regarded as disorders of neuronal hyperactivity, but evidence shows that temporal lobe seizures also cause reduced activity in subcortical arousal nuclei, including cholinergic neurons in the pedunculopontine tegmental nucleus (PPT), a key node of the reticular activating system. The synaptic mechanisms underlying the reduced ictal activity of cholinergic neurons in the PPT are unknown. Whole-cell *in vivo* recordings were made from PPT neurons in head-fixed rats to distinguish active inhibition from withdrawal of excitatory input as the driver of reduced ictal neuronal firing. A subset of PPT neurons exhibited reduced firing and hyperpolarization during seizures and stained positive for choline acetyltransferase. These PPT cholinergic neurons also showed increased input resistance, reduced membrane potential variance and fewer EPSP-like events during seizures. These data weigh against active ictal inhibition and support withdrawal of excitatory input as the dominant mechanism of decreased activity of cholinergic neurons in the PPT.

Acknowledgements

The author thanks his collaborators, without whom this work would not have been possible, including Zongwei Yue, Jun Hwan Ryu, Garrett Neske, and David McCormick. Many thanks to Quentin Perrenoud and Jessica Cardin for helpful suggestions on whole-cell *in vivo* recordings.

A special thanks and unquantifiable gratitude to my mentor, Hal Blumenfeld, for everything—including jumping up and down with me in the lab after I broke into my first neuron.

This work was supported by NIH R01 NS066974, R01 NS096088 (H.B.) and by an HHMI-CURE fellowship (J.A.).

Table of Contents

Introduction

The mechanisms by which subcortical activating networks regulate states of arousal have long been a subject of debate and experimentation, with evidence pointing to the pedunculopontine tegmental nucleus (PPT) as a crucial node in this far-reaching system [1, 2, 3, 4]. Historically, the study of pathologic function to delineate normal physiology has been the rule, rather than the exception, and recent work has shown that PPT neuronal activity is decreased during focal temporal lobe seizures that impair level of cortical arousal [5]. The afferent signaling regulating PPT activity and the mechanisms by which PPT neurons integrate signaling has yet to be clearly elucidated [4].

On a brain-wide scale, prior work has dissected out areas of inhibitory and excitatory activity during seizures [6, 7, 8, 9]. On a cellular level, extracellular recordings have revealed that neurons of specific nuclei exhibit reduced neuronal firing during seizures [5, 10]. In the present study, we delve into the intracellular membrane potential (V_m) level using *in vivo* whole-cell recordings from areas deep in the pedunculopontine brainstem in order to elucidate the synaptic mechanisms underlying ictal changes in neuronal activity of the PPT.

A subset of cholinergic PPT neurons, identified previously[5] using extracellular recording techniques, exhibit reduced firing during focal limbic seizures. How limbic seizures lead to reduced firing of ChAT-positive neurons in the PPT is unknown. Prior studies suggest that the activity of these neurons is likely modified by contributions of both excitatory and inhibitory input [11, 12, 13], however, the afferent synaptic changes resulting in decreased firing can be conceptually dichotomized into either an increase in inhibitory input, or a withdrawal of baseline excitatory input.

Tight-seal whole-cell intracellular recording (WCR) is a powerful tool for investigating membrane properties and synaptic input on individual neurons that has expanded from *in vitro* and slice preparations to the realm of *in vivo* studies [14, 15]. The targeting of deep brain structures and brainstem nuclei has been limited by technical complications of their access, with prior reports removing large sections of brain tissue (e.g. cerebellectomy) in order to patch brainstem neurons [16, 17]. The network of brain circuitry involved in seizures likely extends far beyond areas of canonical seizure activity [5, 9, 10, 18], thus techniques such as slice preparations or *in vivo* studies that involve removal of large swaths of brain are less likely to produce meaningful data regarding distant seizure networks. In addition, the PPT receives afferent input from many different areas of the brain and the functional contribution of each is not well known [4, 19, 20, 21].

In the present study, a minimally invasive technique was used to access deep brainstem nuclei of the rat midbrain tegmentum, with negligible disturbance of brain architecture. In brief, borosilicate patch pipettes were fabricated with a 9-10mm taper and passed through ~200-300µm diameter craniotomies to the area of the pedunculopontine tegmental nucleus (PPT). Using this technique, we attained stable, *in vivo* whole-cell recordings from neurons in the area of the PPT while triggering focal limbic seizures.

The contributions of excitatory versus inhibitory input as regulators of neuronal activity are integral to answering questions regarding mechanisms by which neurons process information [11, 12, 22, 23]. We identified a subset of reduced-firing hyperpolarizing (RfHp) neurons in the PPT, putatively cholinergic by histology. In addition to the RfHP phenotype, these PPT neurons exhibit a rise of input resistance during seizures as well as a reduction in ictal membrane potential variance (σ^2) and reduced frequency of EPSP-like events. Such characteristics could be

explained by a mechanism of reduced excitatory synaptic input on cholinergic neurons in the PPT during seizures.

Statement of Purpose & Hypothesis

The purpose of this work is to describe the synaptic mechanisms underlying the reduced ictal activity of cholinergic neurons in the PPT during focal limbic seizures. The following experiments were performed with the hypothesis is that measures of membrane potential, input resistance and EPSP-like activity will show different patterns ictally compared to baseline, pointing to either active inhibition or a withdrawal of excitatory input as the primary mechanism of reduced neuronal firing rates.

Experimental Methods

All experiments were performed by John Andrews. Zongwei Yue assisted John Andrews with histology and spike-sorting analyses. Matlab data analysis was performed in collaboration with Jun Hwan Ryu. Garrett Neske provided helpful experimental technique advice regarding whole-cell recordings as well as providing protocols for making intracellular solutions.

Animal Preparation and Surgery

All procedures were conducted in compliance with approved institutional animal care and use protocols. A total of 54 female Sprague Dawley rats (Charles River Laboratories) age 6 – 10 weeks, weighing 180 - 275g were used in these experiments. All surgeries were performed under deep anesthesia using a ketamine (90 mg/kg) and xylazine (15 mg/kg) mixture. A summary of the technical aspects of these initial surgeries under deep anesthesia are as follows. The animal was weighed, scalp was shaved, and head was pinned into a stereotactic frame with dual

microelectrode manipulator arms (Kopf Instruments, CA). Scalp was incised and retracted bilaterally to expose underlying tissue and periosteum. Tissue and periosteum were subsequently removed using blunt dissection to expose the dorsum of the skull, including the bregma and lambda sutures. Stereotactic coordinates of these sutures were recorded and used to mark locations for craniotomies over the right lateral orbital frontal cortex (LO), hippocampi (Hc) bilaterally, and bilateral micro craniotomies over the PPT. Stereotactic coordinates are detailed below. Initial craniotomies were made at all locations and dura was left intact to protect underlying brain as long as possible. Craniotomies over LO and Hc were made with a diameter of roughly 1.5-2mm. Electrodes were inserted rostrally to caudally, as such the first to be inserted was the 3-4MΩ tungsten (UEWMGGSEDNNM, FHC) electrode in the LO. Dura, arachnoid and pia were removed immediately prior to electrode insertion using tungsten needles of 1µm tip diameter.

Following initial surgery for electrode implantation, a low-dose ketamine (40 mg/kg) and xylazine (7 mg/kg) mixture was used to produce a state of "light" ketamine/xylazine anesthesia in which slow waves occur less than approximately once per 10 s, but animals remain unresponsive to toe pinch as described previously, prior to induction of seizures in our acute seizure model[5, 9].Stereotactic coordinates of brain structures and nuclei were calculated based on Paxinos and Watson (1998) and were measured in millimeters relative to bregma. Following acute experiments, animals were sacrificed with Euthasol (Virbac). Brains were resected for histological analysis and to verify electrode locations.

LFP and MUA Electrophysiology

Local field potential (LFP) and multiunit activity (MUA) from lateral orbitofrontal cortex (Ctx LFP & Ctx MUA), as well as LFP from hippocampi (Hc) were acquired and amplified as previously described[5, 10]. Briefly, a unipolar, 3-4MΩ tungsten (UEWMGGSEDNNM, FHC) electrode was placed in the lateral orbitofrontal cortex (AP +4.2; ML 2.2; SI -4.0) (Paxinos and Watson, 1998). Twisted bipolar, stainless steel recording/stimulating electrodes (E363-2-2TW-SPC, PlasticsOne) were placed bilaterally in hippocampi (Hc) at anteroposterior (AP) -3.8; mediolateral (ML) ±2.5; superior-inferior (SI) -2.5mm (Paxinos and Watson, 1998). Seizures were induced as described previously[5, 9] in either the right or left Hc, using a 2s, 60Hz square biphasic wave (1ms per phase) Hc stimulus and current amplitude titrated to produce focal hippocampal seizure activity based on polyspike discharges without propagation to frontal cortex. LFP and MUA recordings were amplified using a microelectrode AC amplifier (model 1800 A-M Systems) and broadband filtered from 0.1Hz to 10 kHz (x1000 gain). A model 3363 Krohn-Hite filter was used to low-pass filter LFP at 0.1 - 100Hz and high pass filter MUA at 400Hz – 10kHz[5, 8, 9]. A Micro1401 (CED) A/D converter was used with a sampling rate of 1,000 Hz for Ctx LFP, 25,000 Hz for Ctx-MUA, 1,000 Hz for Hc LFP, and 25,000 Hz for whole-cell recordings of PPT neurons (below). Continuous recordings were made using Spike2 v8.06 (CED) software.

Whole-cell recordings

For whole-cell recordings from PPT we modified procedures used previously for WCR from more superficial targets (Neske et al., 2015). Care was taken to make craniotomies over the PPT as small as possible to enable the skull and dura to stabilize the brain, but just large enough to allow the micropipettes to pass. The PPT was targeted at coordinates (relative to bregma) AP -

7.8; ML ±1.8; SI 7.0 mm. The skull was thinned in a ~1mm diameter depression at the craniotomy target using a hand drill and tungsten microneedles were then used to carefully dissect a 200-300 µm craniotomy from the thinned bone under a microscope to expose the underlying dura. A saline bath was then constructed around the craniotomy using dental cement, and the dura and pia were carefully removed using tungsten needles of 1µm tip diameter (10130-05, Fine Science Tools) prior to micropipette insertion. The saline bath was made around the craniotomy to serve as a reservoir communicating with the cerebrospinal fluid in which to put the Ag-Cl reference electrode.

A potassium-gluconate-based intracellular solution was used for micropipettes with a composition consisting of 130mM K-gluconate, 0.2mM EGTA, 4mM KCl, 2mM NaCl, 10mM HEPES, 4mM ATP-Mg, 0.3mM GTP-Na, 14mM phosphocreatine-2K, 0.5% Biocytin and titrated to a pH of 7.25 and 290 mOsm (Neske et al., 2015).

One aspect limiting the depth of whole-cell recordings is reproducible creation of long, narrow glass pipets with sufficiently low resistance. This problem was solved by using an extra-wide, 2.5 x 4.5mm filament in a P-1000 micropipette puller (Sutter Instruments) and creating a multi-line program with 1 high velocity line followed by 3 low velocity lines while keeping pull, heat, time and pressure settings constant. Borosilicate glass (1B150F-4, World Precision instruments) of outer diameter 1.5mm and inner diameter of 0.84mm was used to make pipets with this multi-line program. Pipets were produced to have a long 9-10mm taper to allow recordings deep below the cortical surface, and a resistance of 3.5 – 6 MΩ.

Even in the most optimal state of the pipette pulling program, only 1 in 4 to 1 in 5 pulls resulted in pipettes meeting the standard of 3.5 – 6 MΩ. There may be variation of many MΩ between pipettes pulled from different pulls, even run through the identical program. This is

because there is a very narrow window of parameters that will produce a pipette to have a 9-10mm taper while retaining a low resistance tip. Visual inspection and microscopic measurement of tip diameter can provide some information about the tip resistance, but experience has shown this to be unreliable in the context of these very long, tapered pipets where a not insignificant portion of the resistance may be from the long, tapered path. The best way to definitively test the resistance of any pipette is to fill it with a solution, insert it into a bath and run current through the pipette to the reference electrode. This pipette may not be withdrawn from a solution once it is inserted because the contaminants on the surface film of the liquid will contaminate the tip. Because the tip of a pipette must not be contaminated in order to form a giga-seal with a neuron, one cannot test the resistance of any particular pipette before actually using it. If one were to try every pipette during each experiment one would end up using 4-6x the intracellular solution as if every pipette were usable. This testing every pipette at the time of the experiment is also hugely time-intensive in the context of an experiment that takes ~16 hours at a time when things run smoothly. Thus, the problem was addressed in the following manner.

When a glass capillary is pulled, it is pulled from both ends with the heat filament in the middle, resulting in a pair of two pipettes for each pull, referred to from here on as “twins.” Moreover, these twin pipettes saw the exact same parameters and experienced the same break to result in their tips. Thus, the twin pipettes should have very similar resistances. This was confirmed over many trials (data not shown). In light of this, when pulling pipettes the day prior to an experiment, the pipettes were separated so that the pairs to which they belong is identifiable. One pipette from each twin-pair was filled with saline, attached to the head stage with the electrode, and lowered into a saline bath that also contained the reference electrode. A current was run through the electrodes and a resistance of the pipette was calculated. This was

done for one of each twin-pair, so that approximations of the resistance of the other twin in the pair were attained. Only the pipettes with twins whose resistances were within the specified range were used on the day of the experiment. This greatly reduced the amount of intracellular solution used during each experiment and increased the ratio of usable to non-usable pipettes at the time of the experiment.

Regarding the technique of pipette insertion into the brain of an animal, the first pipette lowered into the craniotomy down to the target region was used to create a micro-canal through which subsequent pipettes might pass with less likelihood of damage/contamination of the tip. This pathfinder pipette contained saline, was under 0 mbar intrapipette pressure and was only lowered until 150 µm superficial to the target region—all of these changes were made in order to minimize damage to surrounding tissue and the target region while making the micro-canal. The pathfinder pipette was left in place for 25 minutes under no pressure to allow formation of the micro-canal. To prevent contamination of subsequent recording pipette tips during descent into the brain, 500mbar positive intrapipette pressure was maintained throughout the 30-50 µm/s descent to target region. Once at the most ventral aspect of the PPT, pressure was lowered to 24-28mbar and descent slowed to ~1 µm/s.

A thin rubber tubing system was custom made to connect to the space in the electrode holding head-stage proximal to the glass pipet, such that pressure in the glass pipet could be measured and controlled. This tubing had another end attached to an electric manometer (EXTECH, item# 407910) as well as a three-way stopcock with an opening to which a syringe or mouthpiece could be attached. In this way, air could be introduced into the closed system to increase the intra-pipette pressure to protect the pipette tip, as well as carefully titrate the pressure while searching for neurons.

Recordings were made using a Multiclamp 700B (Axon) amplifier and digitized at 25kHz using a Micro1401 (CED) and Spike2 v8.06 (CED) software. The neuron-searching step of acquiring WCR was undertaken in voltage-clamp mode, using 5mV 50Hz 10 ms voltage steps with current response visualized in real-time both in Spike2 software and on an external oscilloscope for blind-patching.

In search mode, the experimenter would watch the square current response (inversely related to resistance) to the 5mV 50Hz 10 ms voltage steps on the oscilloscope, looking for changes indicative of a pipette juxtaposed to a neuron. While *in vitro* patch clamping protocols have described the visualization of this peri-neuron change as a sudden, sustained increase in resistance (i.e. decrease in current response), neurons *in vivo* do not show this static signature. The signature of being next to a neuron *in vivo* with a patch pipette is best described as a rapid, flapping oscillation in current-response. One explanation for this flapping, or fluttering signal is the heartbeat of the animal causing microscopic movements of these single neurons relative to the more stable pipette and micromanipulator apparatus, with the neuron covering and then uncovering the pipette tip in rapid sequence. In the experience of this experimenter, the best way to proceed is to advance the micromanipulator an additional 1µm immediately after first encountering this a neuron in this manner. If the signal stops, then it is likely the pipet tip was not in optimal position to form a tight seal with the neuron, and searching may continue as long as the intrapipette pressure (24-28mbar in search mode) was not released. If following this 1µm advance, the flapping signal either enhances or continues as is, then within 5-10s the experimenter should release the positive pressure (open stop-cock to air) and observe the subsequent current response for evidence of forming a seal with the membrane. Evidence for a seal forming are an immediate drop in current response such that the signal on the oscilloscope

drops to what appears as a thin, straight line, despite the 5mV voltage steps continuing. The Axon MultiClamp 700B Commander software interface allows for the experimenter to calculate real-time resistance from voltage steps for. Ideally, the resistance will rise to over 1 GΩ immediately after releasing positive pressure. It is best if magnitude of resistance is learned to be evaluated by sight-reading of the oscilloscope wave-form, so that calculations need not be made on the fly. If the resistance rises substantially, but is still in the hundreds of MΩ immediately after release of positive pressure, very gentle negative pressure should be applied through the mouthpiece connected to the stop-cock tubing system (-8 to -13mbar). This may facilitate formation of the giga seal. Another adjunct for seal-formation is clamping the pipette voltage to a hyperpolarized potential (e.g. -60mV). The best seals form immediately, but viable seal may also mature over the course of ~ 1 minute. In the experience of this experimenter a seal is unlikely to form after several minutes of having not formed an adequate seal.

Once a seal is formed with the neuron, in order to rupture the patch of membrane circumscribed by the tip of the pipette either brief oral suction, or a current pulse were applied. If successful, whole-cell configuration was evidenced by a change in the current-response on the oscilloscope from the flat, minimal response of a giga-seal to the sharp rise and exponential decay indicative of having access to the interior of a neuron with the cell membrane acting as a capacitor to produce such an RC charging curve. If neither of these break-in strategies were successful in isolation, when applied at the same time they sometimes met with success.

As mentioned in the Results section, of 295 electrode passes, 36 neurons were recorded from, a success rate of ~10%, and of these approximately half were recovered histologically. The 295 electrode passes include only pipettes with the appropriate resistance (3.5 – 6 MΩ, measured upon lowering into the bath) and which were lowered into the craniotomy without adverse event.

The majority of failed passes occurred either while searching for neurons in the target region or at the step of forming a gigaseal. Increases in pipette tip resistance of >20% while in search-mode were interpreted as a clogged pipette tip and the pass was abandoned and pipette removed, accounting for roughly 50% of failures. Most of the remaining 50% of failures were at the step of forming a gigaseal, where a gigaseal did not fully form upon release of positive pressure and application of gentle (~10-15mbar) suction by mouth, despite being preceded by the fast-fluctuating tip-resistance profile characteristic of a neuron positioned at the tip of one's pipette. Other failures include forming a gigaseal and then failing during the brief suction pulses to attain whole-cell configuration, or upon attaining an RC charging profile consistent with WCR, the neuron would begin firing uncontrollably and die. In addition, there were several instances of breaking into whole-cell configuration, but the RC charging curve demonstrated high initial access resistance, which could not be remedied through further suction or manipulation. Initial access resistance was measured in voltage clamp upon attaining whole-cell configuration. Cells were discarded if initial access resistance was above 70 MΩ. Recordings were conducted in current clamp mode soon after attaining WCR and the bridge was balanced in current clamp mode periodically throughout recordings. If bridge balance rose above 70 MΩ during recordings, intracellular data regarding resting potential changes and subthreshold fluctuations in membrane potential during baseline vs. seizures were discarded.

After attaining a stable whole-cell recording from a neuron in PPT, focal hippocampal seizures were induced using the protocol described above[5, 9]. Moment-to-moment input resistance was measured in some neurons in current clamp using 20 - 30pA, 50 or 100ms hyperpolarizing current steps at 5 or 10Hz before, during and after seizures. At the conclusion of recordings, animals were euthanized and perfused for histology.

Histology

Brains were fixed with 4% paraformaldehyde and cut in 60µm slices for histology. Brains were then stained for biocytin cy3-streptavidin construct and co-stained using an antibody to Choline-acetyltransferase (ChAT) as previously described in detail[5]. A Zeiss LSM 710 Duo NLO/multiphoton confocal microscope with a C-Apochromat 40x/63x/1.2 W Corr objective was used for imaging.

Data Analysis

Data analysis was performed using Spike2 (CED, v5.20a), and in-house software written on MATLAB (R2009a, Mathworks). Analysis epoch were defined as follows: 1. Baseline: 20–0 s before stimulus; 2. Ictal: the first 20 s of hippocampal seizure activity (or the entire period of seizure activity where indicated), based on large amplitude, polyspike activity in the hippocampal LFP recordings; 3. Postictal: 0–20 s after seizure; 4. Recovery: 20 s following the postictal period. Analyses were performed only on neurons identified by intracellular staining as well as one RfHp neuron that was not histologically recovered. In addition, all included neurons had RC charging curve compatible with transition to intracellular recordings, access resistance <70 MΩ, exhibited reproducible action potentials, and stable resting potential. Note that one RfHp and one non-RfHp cell were excluded from V_m, EPSP-like event, variance and Rin analyses due to access resistance >70 MΩ. One non-RfHp neuron exhibited artifact from pulse-subtraction (of current-steps for R_{in} measurement) and thus was also excluded from V_m, variance and EPSP analyses requiring such subtraction.

Statistics were calculated using MATLAB, Excel and Graphpad Prism software. Repeated-measures ANOVA and two-tailed student's t-tests were used, paired where appropriate, with cut-off for statistical significance of $p < 0.05$. Significance is corrected for multiple comparisons where appropriate using the Holm-Bonferroni method.

Neuronal spiking rate analysis. Spike sorting on the WCR recordings was performed in Spike 2 using template-matching based on waveform shapes to identify single units. Raster plots of neuronal firing were generated for each neuron, and then histograms of mean firing rate were calculated across neurons in 1s non-overlapping bins for each epoch (Figures 2, S3).

V_m hyperpolarization during seizures vs. baseline. To calculate amplitude of membrane potential hyperpolarization during seizures, membrane potentials in baseline and ictal epochs were averaged in 3s bins after excluding the 20ms period surrounding each action potential (5ms prior, 15ms following) and subtracting pulses from those neurons receiving them as described below. The bin just prior to seizure stimulation (within the baseline period) was compared to the bin of most negative membrane potential during the ictal period. The difference between the baseline bin prior to seizure onset and the ictal bin with the most negative membrane potential is reported as the amplitude of ictal hyperpolarization.

Input resistance (R_{in}). Input resistance was measured by delivering repeated hyperpolarizing square current pulses and measuring the change in membrane potential for each step, as resistance (R) is related to change in voltage (ΔV) and current (ΔI) through Ohm's law $R=\Delta V/\Delta I$. Square hyperpolarizing pulses were delivered at a constant frequency and amplitude during the

recording of each neuron, either at 5 or 10Hz (100ms or 50ms pulse duration) with amplitudes of -30 or -50pA (Figure 6A). ΔV was calculated in Spike2 by taking the mean V_m during the last 25ms prior to each positive or negative step (when voltage had reached steady-state) and taking the difference between mean V_m in all pairs of these 25ms epochs. Current steps overlapping within 5ms prior to or 15ms following an action potential were discarded. R_{in} measurements within individual neurons were compared from the 20s baseline epoch prior to seizure onset, to those during the entirety of the ictal period, and the 20s recovery epoch beginning 20s following cessation of hippocampal ictal activity, using a two-tailed t-test (Figure 6C, D). Time course graphs of mean ictal changes in R_{in} were constructed using 3s bins of R_{in} data (Figure 6B). Because one seizure in one RfHp neuron was significantly longer than all comparison seizures in both RfHp and non-RfHp neurons with pulses, later bins from that seizure extending beyond other ictal periods were not included in the graphical time course analysis, although all ictal values were included for R_{in} analyses in 6C and 6D. Normalization to baseline R_{in} was carried out by calculating the mean R_{in} for the 20s prior to seizure onset, and then dividing all R_{in} values for the 3s bins by the mean baseline R_{in}.

Analysis of EPSP-like events and voltage histograms. Prior to analysis of EPSP-like events, hyperpolarization and voltage histograms, we first removed the exponential RC pulses from neurons in which repeated 5 Hz or 10 Hz current steps were applied to measure R_{in}. This was done by obtaining an average RC pulse signal for each such neuron during the baseline and ictal periods, and then subtracting these average pulses from the raw signal. This procedure effectively and smoothly removed the pulse artifacts from all neurons except for one non-RfHp neuron, which was therefore excluded from these analyses.

EPSP-like events were identified in MATLAB as positive fluctuations in membrane potential of >0.4mV with a rise-time of <2ms [24, 25], excluding the time periods from 5 ms before to 15 ms after any action potentials (Figure 6E). Mean amplitude and frequency of EPSP-like events were then calculated for the baseline (20s before seizure onset) and full ictal periods.

To investigate the variance of voltage distributions before, during and after seizures, we again excluded signal from a 20ms block around action potentials (5ms prior and 15ms after), subtracted pulses from pulsed neurons and then high-pass filtered (>0.5Hz) the V_m signal for these epochs to remove slow drift and select for higher frequency fluctuation. Variance was then calculated from the resulting membrane potential values and the mean σ^2 values were compared using paired two-tailed t-tests. To graphically depict the distribution from which this membrane potential variance was calculated, we created histograms of the voltage values during the Baseline (0 to 20s before seizure onset), Ictal (entire ictal period) and Recovery (20 to 40 s after seizure end) epochs. We fit the histogram with a Gaussian curve to center the histograms to the mean of the fitted Gaussian. Each histogram was normalized by the maximum height and the resulting histograms were summed across neurons, with equal weight. The final histogram was normalized again by dividing the values by the maximum height (Figure 6F, G).

Results

Reduced-firing, hyperpolarizing neurons of the PPT

The present study aims to find the mechanism underlying a reduction in firing rate observed in cholinergic neurons in the PPT [5]. To this end, established techniques for *in vivo* patch clamping were modified (see Methods) and combined with a rat model of focal limbic seizures that impair

level of cortical arousal [5, 8, 9, 26] so as to attain whole-cell recordings from neurons in the area of the PPT during seizures.

Whole-cell configuration was attained from 36 neurons in the stereotactic area of the PPT, after a total of 295 pipette passes into the brains of 54 rats. 5 neurons showed a distinct phenotype of reduced firing and hyperpolarization (RfHp), as seen in Figure 1A, and are the focus of this study. 4 out of 5 of these RfHp neurons were histologically recovered by identifying neurons filled with biocytin (from the intracellular solution within the WCR pipette) using a fluorescent streptavidin construct and co-staining for choline-acetyltransferase (ChAT) using immunohistochemistry. All recovered RfHp neurons (4 of 4) expressed ChAT positivity (figure 1B), whereas none of the recovered non-RfHp neurons (0 of 12) were ChAT positive ($P<0.001$, Fisher's exact test). An example of a non-RfHp, non-ChAT neuron is shown in Figure 2B, and the locations of all histologically recovered neurons are shown in Figure 3.

Figure 1

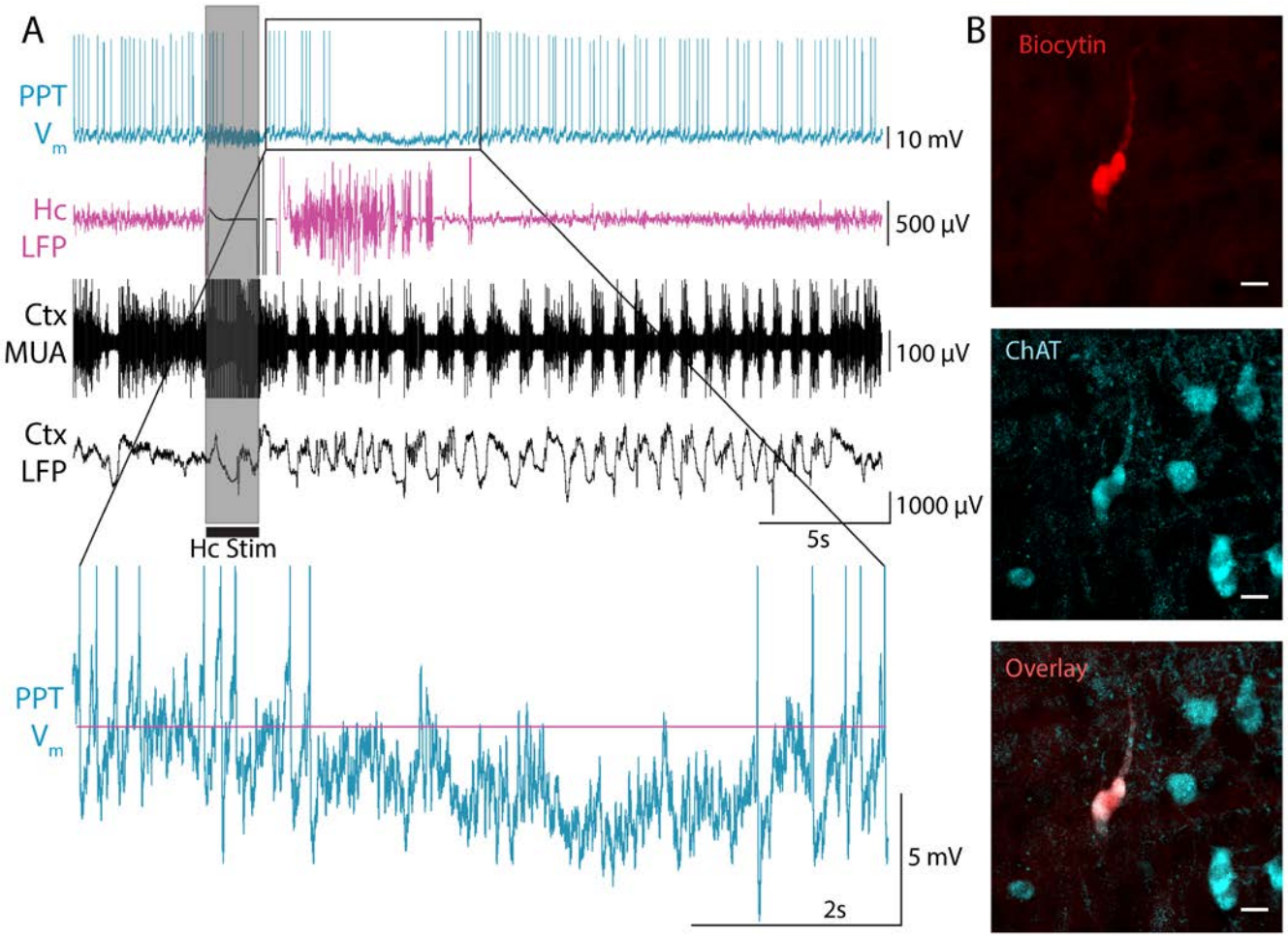

Figure 1. Reduced-firing hyperpolarizing (RfHp) neuron in the pedunculopontine tegmental nucleus (PPT) during a focal limbic seizure. (A) Whole-cell current clamp recording of membrane potential (Vm) in PPT neuron shows reduced firing and hyperpolarization (see inset) during a focal seizure induced in the hippocampus by a 2s, 60 Hz stimulus (gray bar). Concomitant recording of local field potential (LFP) shows polyspike seizure activity in the hippocampus (Hc). Orbital frontal cortex (Ctx) LFP exhibit slow-waves and multiunit activity (MUA) recordings show Up/Down state firing at seizure onset lasting into the postictal period. (B) Histology demonstrates co-localization of biocytin (from intracellular electrode solution) staining and ChAT immunohistochemistry for neuron recorded in A. Scale bar is 20 microns.

A representative whole-cell recording from an RfHp neuron in PPT is shown in Figure 1 A. As seen in the top trace in cyan, prior to seizure initiation the neuron exhibits a continuous

firing pattern. Hippocampal local field potential (Hc LFP) is shown in the pink trace second from the top with frontal cortical multiple unit activity (Ctx MUA) and cortical LFP (Ctx LFP) in the bottom black traces. Following hippocampal stimulation (Hc stim, gray bar), high amplitude seizure activity is seen localized to the hippocampus. In addition, there is a sharp transition from low-voltage fast activity with sparse slow waves in cortical LFP to synchronized cortical slow waves and MUA Up/Down firing states at the time of seizure onset as reported previously [5, 9]. Concomitant with seizure onset, the PPT neuron's

Figure 2

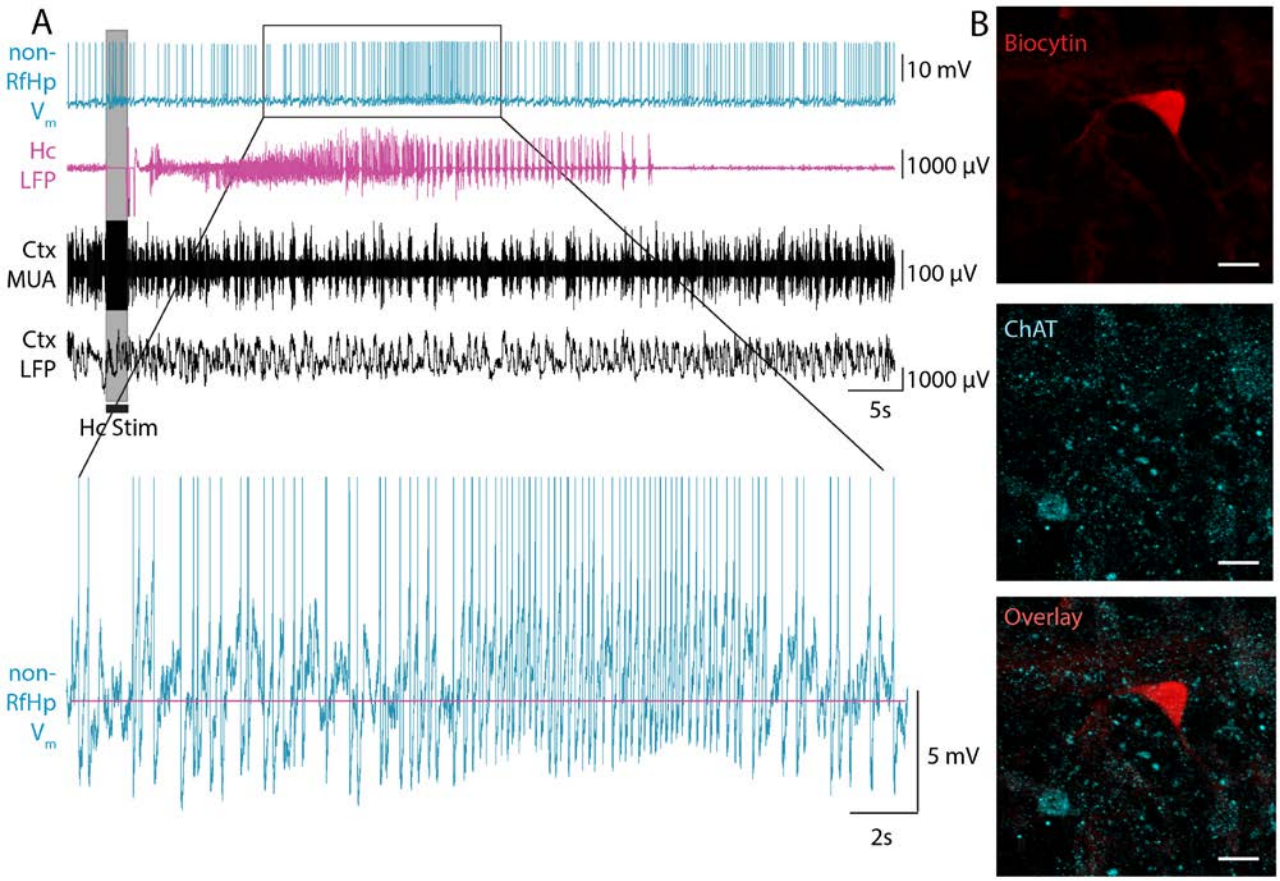

Figure 2. Non-RfHP neuron in the pedunculopontine tegmental nucleus (PPT) during a focal limbic seizure. (A) Whole-cell current clamp recording of membrane potential (Vm) in PPT neuron shows continued tonic firing and no significant hyperpolarization of the resting membrane potential during a focal seizure induced in the hippocampus by a 2s, 60 Hz stimulus (gray bar). Concomitant recording of local field

potential (LFP) shows polyspike seizure activity in the hippocampus (Hc). Orbital frontal cortex (Ctx) LFP and multiunit activity (MUA) show slow-wave and Up/Down state activity during and following the seizure. (B) Histology demonstrates biocytin staining (from intracellular electrode solution) but no ChAT staining by immunohistochemistry staining of the recorded neuron from A. Scale bar is 20 microns.

firing tapers off and is silenced for the majority of the seizure before resuming a regular firing pattern as the seizure ends. The expanded view of the cyan whole-cell recording of the PPT neuron during the seizure shows a hyperpolarization of roughly 5mV at its nadir over the course of the seizure before resuming firing at the seizure's end. In comparison, non-RfHp neurons recorded from the same region did not show reduced tonic firing or hyperpolarization during seizures (example shown in Figure 2). Figure 1B shows the biocytin-filled RfHp neuron (same neuron as Figure 1A), which stained positive for choline-acetlytransferase like all other histologically-recovered RfHp neurons (Figure 3). This finding is consistent with the notion that these are the same subset of neurons previously identified in the PPT and shown to consistently reduce their firing during seizures [5].

The action potential firing of RfHp neurons before, during and after focal seizures is depicted in the raster plots in Figure 4A. Histograms in Figure 4B present the average firing rate in 1s bins over the course of each 20-second epoch. Baseline rate of firing varied among neurons, but there was a consistent reduction in firing rate during the ictal period relative to baseline with a mean of -51.6% (SEM 12.8%, P = 0.016).

Non-RfHp, ChAT-negative neurons showed moderately variable responses as expected for this heterogenous group of neurons [4], trending toward increased rates of firing during the ictal period (Figure 5) with a mean change relative to baseline of +465.9% (SEM±192.2%, P = 0.096).

Figure 3

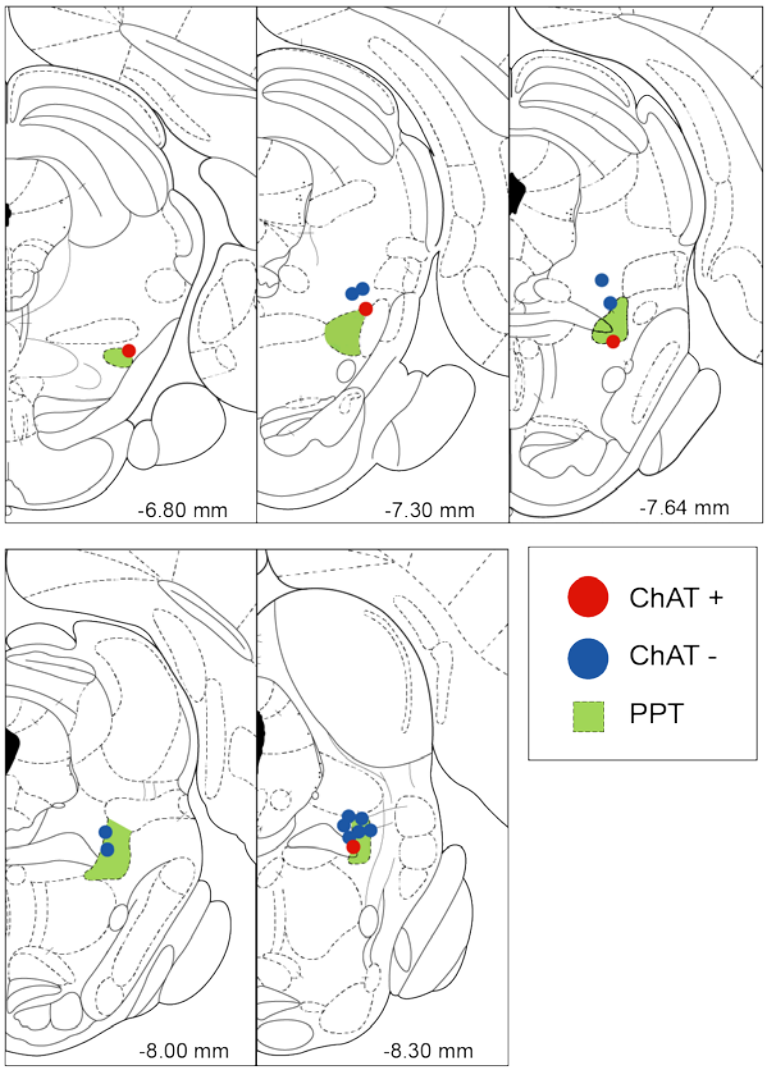

Figure 3. Anatomical locations of histologically recovered neurons. 16 neurons were recovered in the region of the pedunculopontine tegmental nucleus (PPT) based on biocytin staining following whole-cell recordings. Red dots indicate the 4 reduced firing hyperpolarizing (RfHp) neurons that were recovered, all of which were verified to be choline acetyl transferase (ChAT)-positive. One RfHp neuron was not histologically recovered. Blue dots indicate the 12 histologically recovered non-RfHp neurons, all of which were ChAT-negative. AP coordinate of coronal sections are in millimeters relative to bregma. Schematics taken with permission from Paxinos and Watson, 1998.

Having demonstrated reduced-firing in a subset of putatively cholinergic PPT neurons using whole-cell *in vivo* recordings from the PPT in a model of focal hippocampal seizures, the

next step was to interrogate the intracellular properties of these neurons that might offer clues as to the mechanism of reduced firing. One aspect visible on the expanded WCR trace from Figure 1 is the hyperpolarization—all RfHp neurons exhibited an ictal hyperpolarization relative to baseline pre-ictal membrane voltages. The mean membrane potential of RfHp neurons during the 20s baseline prior to seizure onset ranged from -53.73mV to -64.67mV (SEM±2.13), adjusted for junction potential. The average amplitude of ictal hyperpolarization for RfHp neurons was -3.82mV (n=4, SEM±0.81, P=0.026) relative to the pre-ictal baseline membrane potential. In contrast, for non-RfHp neurons, the most hyperpolarized ictal V_m during seizures was on average no different than baseline: +0.85mV (SEM±0.43, n=10, P = 0.097).

Figure 4

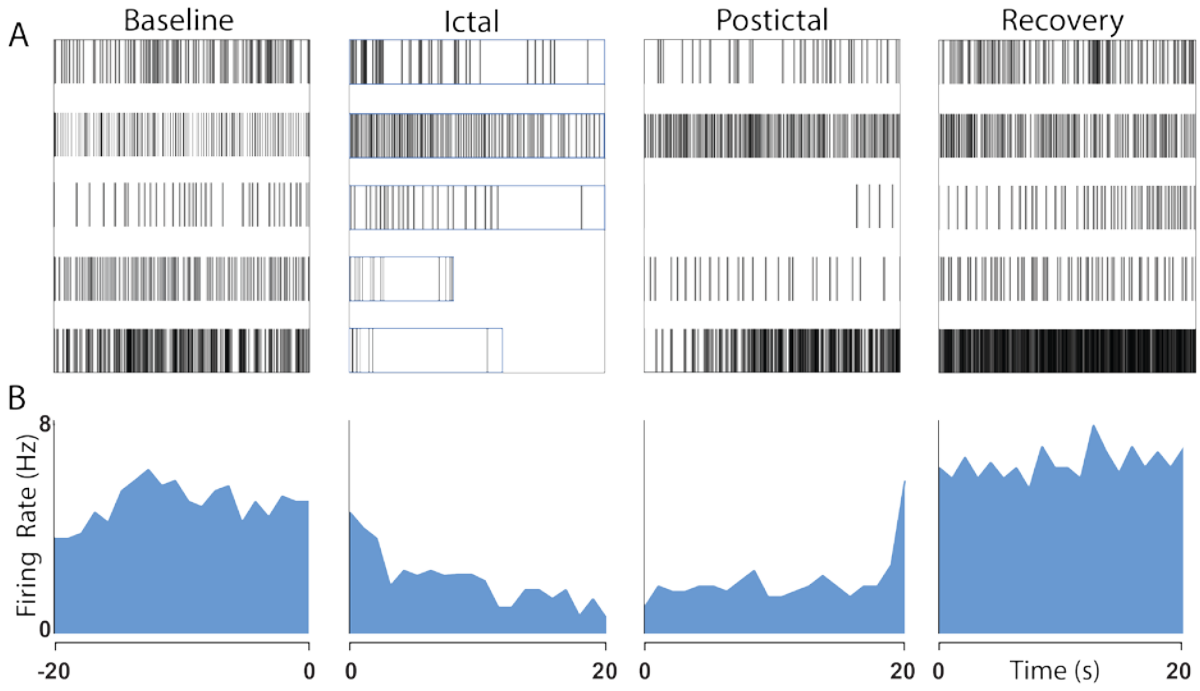

Figure 4. Reduced action potential firing in RfHp neurons during seizures. (A) Raster plots (five cells from five animals) show decreased firing during the Ictal period compared with Baseline. Boxes in ictal panel indicate duration of seizures up to the first 20 s. (B) Histograms of firing rate in 1 s bins across neurons. Mean reduction in firing rate of Ictal compared to Baseline epochs was -51.6% (SEM 12.8%, P = 0.016, paired t-

test). Baseline is defined as the 20 s preceding seizure onset. Ictal is defined as up to the first 20 s following seizure onset. Postictal is the first 20 s following seizure end. Recovery is the 20 s following the Postictal period.

Figure 5

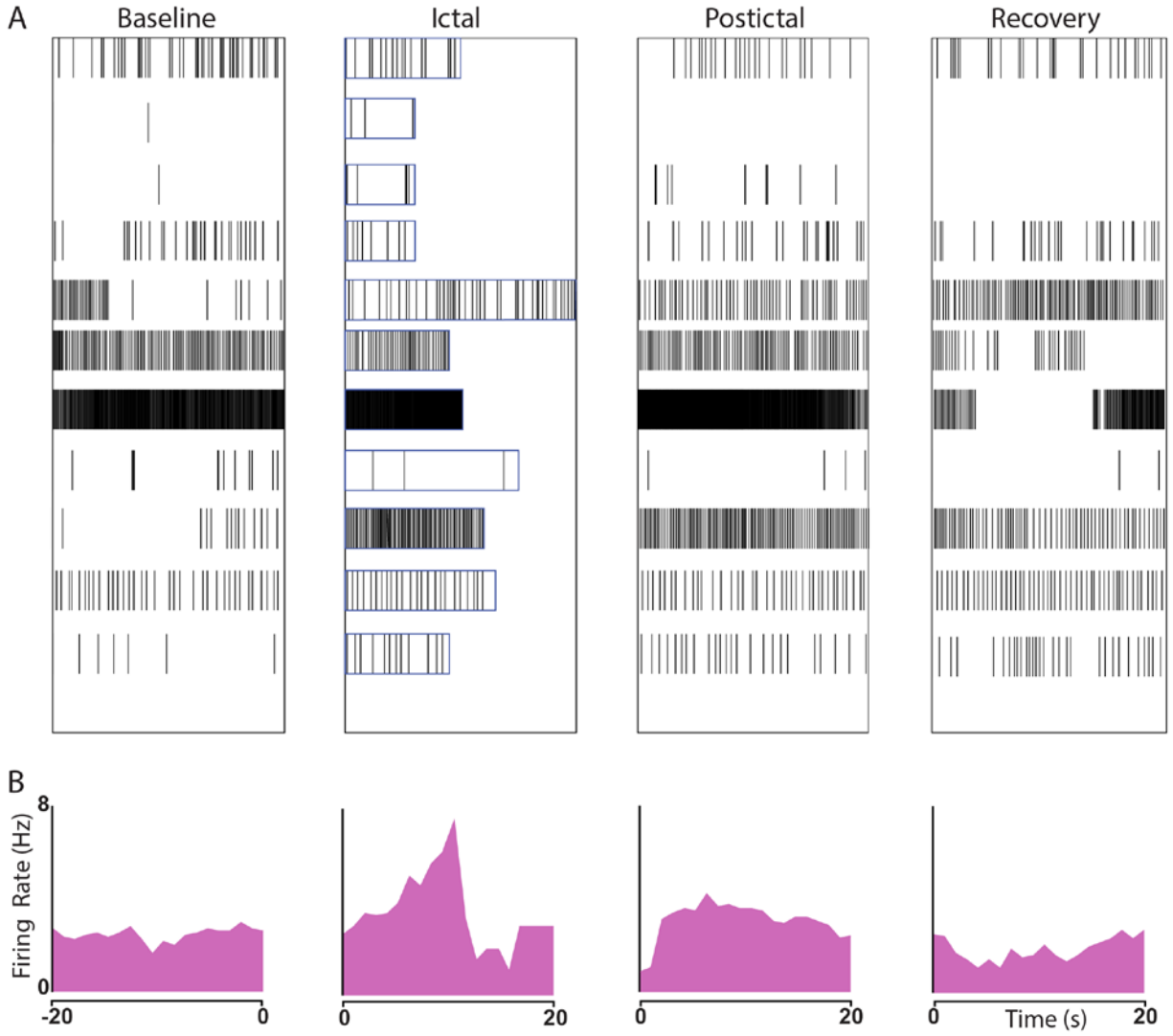

Figure 5. Non-RfHp neurons showed variable pattern of firing during seizures. (A) Raster plots of 12 cells from 10 animals show variable pattern firing during the Ictal period with an overall increase compared with Baseline. Boxes in ictal panel indicate duration of seizures up to the first 20 s. (B) Histograms of firing rate in 1 s bins across neurons. Mean change in firing rate trended upward during Ictal periods compared to Baseline, with high levels variation among non-RfHp neurons resulting in no statistically significant mean change (+465.9%, SEM 192.2%, P = 0.096, t-test). 1 non-RfHp neuron showed no action potentials during the Baseline, Ictal, Postictal and Recovery periods, represented by the blank base at the bottom of part (A). Baseline is 20 s prior to seizure

onset. Ictal is the first 20 s following seizure onset. Postictal is the first 20 s following seizure end. Recovery is the 20 s following the Postictal period.

Input resistance and voltage fluctuation during seizures

Dichotomizing the mechanistic options underlying a phenotype of reduced firing and hyperpolarization offers two simplified extremes: active inhibition versus a withdrawal of baseline excitatory input. During active inhibition, for example through increased GABAergic input, one would expect to see a reduction in a neuron's input resistance [12, 27].

Because the RfHp neurons were electrophysiologically identified by properties measurable in current-clamp mode, experiments were continued in current-clamp with the addition of low-amplitude, continuous, square current-steps to measure moment-to-moment input resistance. Input resistance was chosen as a non-specific marker of channels opening and closing. While input resistance lacks the specificity to distinguish between excitatory and inhibitory currents, it offers the experimental advantage of being measurable while the neuron is functioning at physiological membrane potentials and without compromising data-rich current-clamp recordings.

3 RfHp neurons and 4 non-RfHp neurons were recorded with repeated brief current pulses to quantify input resistance before, during and after seizures. Figure 6A shows a current-clamp recording of an RfHp ChAT-positive neuron while 30pA 50ms current pulses are delivered at a rate of 10Hz. Spikes seen in the baseline (black) trace of Figure 6A are truncated to allow an expanded view of the V_m response to current steps (and action potentials were excluded from analysis; see Methods). The ictal trace (cyan) shows reduced firing and hyperpolarization characteristic of the RfHp neurons. As illustrated in the expanded overlay of voltage responses to square current steps, the ictal period of RfHp neurons is accompanied by an

Figure 6

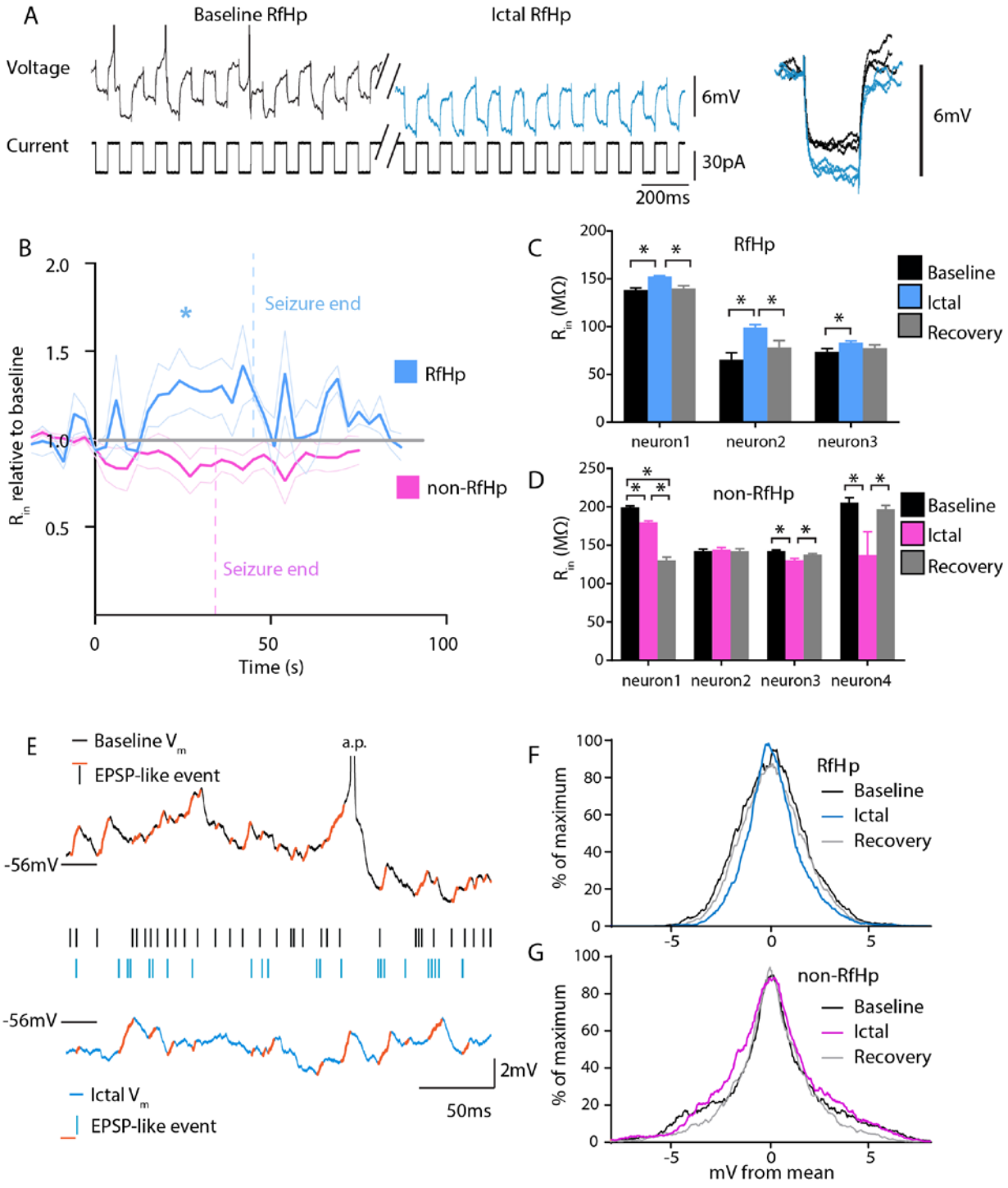

Figure 6. Increased input resistance and reduced membrane potential fluctuations in RfHp neurons during seizures.

(A) Example of response to continuous 10Hz 30pA square current pulses in an RfHp neuron (top trace, Voltage; bottom trace, Current). Action potentials are truncated. The

trace shows reduced firing and hyperpolarization in the ictal period (cyan), as well as a larger magnitude of V_m response to constant current steps, indicating an increase in ictal input resistance. Inset on right shows expanded view of baseline (black) and ictal (cyan) V_m responses to current pulses, with resting potentials aligned vertically to enable differences in response amplitude to be compared more easily.
(B) Mean time course of relative input resistance (R_{in}) during seizures reveal that RfHp neurons (cyan) showed a significant difference from mean baseline and from non-RfHp neurons during the ictal period (* $P<0.05$, two-factor ANOVA). Seizure onset was at time 0, and ends of seizure epochs are indicated by vertical dashed lines for RfHp (cyan, n=3) and non-RfHp (pink, n=4) neurons. Traces show mean R_{in} relative to (divided by) baseline with standard error of mean (SEM).
(C, D) Changes in input resistance (R_{in}) for individual RfHp and non-RfHp neurons. RfHp neurons (C) show consistent increases in R_{in} during the ictal period compared to baseline, whereas none of the non-RfHp neurons (D) show an increase in R_{in} during seizures. Mean and SEM are shown across each neuron that received current pulses (* $P < 0.05$, paired, two-tailed t-test).
(E) Examples of EPSP-like events defined as positive fluctuations in membrane potential of >0.4mV with a rise-time of <2ms [24, 25]. Top (black) trace shows the baseline V_m of an RfHp neuron, while the lower (cyan) trace shows ictal V_m of the same RfHp neuron. Orange markings overly areas meeting criteria for EPSP-like events, with each event also marked as a black (baseline) or cyan (ictal) tick-mark for easier comparison of relative frequency. In group analysis, frequency of EPSP-like events was significantly decreased during the ictal periods of RfHp neurons compared to baseline (see text).
(F,G) Average membrane potential histograms for RfHp neurons (n=4) (F) and non-RfHp neurons (n=10) (G) in the Baseline, Ictal and Recovery periods. Mean histogram for RfHp neurons was narrower for the ictal period (cyan), and the corresponding membrane potential variance of RfHp neurons was significantly decreased during seizures compared to baseline (see text for statistics).

increase in magnitude of voltage response to constant current pulses, indicating an increase in input resistance.

The mean time course of input resistance fold-change during seizures is shown for RfHp vs non-RfHp neurons in Figure 6B. The RfHp curve deflects upward during the ictal period, indicating higher input resistance during the ictal period. This contrasts with the slightly downward deflecting curve of the non-RfHp neurons. The RfHp curve was significantly different from its own baseline ($P = 0.001$, two-factor ANOVA) in addition to differing from the non-RfHp curve during the ictal period ($P = 3.98e-10$, two-factor ANOVA). Input resistance changes

for individual RfHp and non-RfHp neurons are shown in Figure 6C, D. 3 of 3 RfHp neurons showed a significant (P = 4.53e-9, P = 4.05e-5, P = 0.015; neuron 1, 2, & 3 respectively, baseline vs ictal; paired two-tailed t-test) increase in mean input resistance during the ictal phase, whereas 0 of 4 non-RfHp neurons exhibited significant ictal increases in input resistance (P = 0.029, Fisher's exact test). Because hyperpolarization could potentially contribute to changes in input resistance due to closure of voltage-gated ion channels, we repeated the input resistance measurements in 2 of the RfHp neurons both during seizures, and in non-ictal periods (one prior to seizure onset, one following seizure end) in which the membrane potential was hyperpolarized to the same voltage measured during the ictal period (data not shown). In both instances, ictal input resistance was still significantly higher than these non-ictal periods with comparable hyperpolarization, suggesting that the change in input resistance observed ictally is not fully explained by hyperpolarization.

As additional means of evaluating changes in synaptic input during the ictal vs. interictal periods, we examined EPSP-like events and membrane potential fluctuations at baseline and during seizures (Figure 6E-G). While definitive identification of EPSP's is difficult without voltage-channel blockers in the recording solution or a timed stimulus to follow, EPSP's have been described in detail morphologically [24, 25]. We interrogated our data for positive deflections of >0.4mV in a time-frame of <2ms [24, 25] to look for discrete EPSP-like events within our current clamp data—excluding action-potentials and subtracting out current-steps, and compared the baseline to ictal periods (Figure 6E). The frequency of EPSP-like events was significantly decreased during the ictal periods of RfHp neurons compared to baseline (mean Baseline frequency: 97.6 Hz, SEM±20.7; mean Ictal frequency: 88.7 Hz, SEM±19.0; n=4; P = 0.022 paired, two-tailed t-test). Mean amplitude of EPSP-like events in RfHp neurons was not

significantly different between baseline and ictal periods (mean Baseline amplitude: 0.59mV, SEM±0.07; mean Ictal amplitude 0.55mV, SEM±0.04; n=4; P = 0.113 paired, two-tailed t-test). Non-RfHp neurons showed no consistent or significant differences between frequency or amplitude of EPSP-like events in the ictal period compared to baseline (data not shown).

We also plotted the distribution of membrane potential fluctuations at baseline compared to during seizures (Figure 6 F, G). After high pass filtering for signal over 0.5Hz to account for slower changes in membrane potential documented during seizures, the mean membrane potential variance of RfHp neurons was decreased during seizures (mean σ^2=1.79 mV^2, SEM±0.48) compared to baseline (mean σ^2±2.64 mV^2, SEM 0.52, n=4; P = 0.003 paired, two-tailed t-test). In contrast, the membrane potential variance in non-RfHp neurons tended to increase during seizures (mean σ^2=2.15 mV^2, SEM±0.40) compared to baseline (mean σ^2=1.64 mV, SEM±0.53) but was not statistically significant (n=10; P = 0.213). These changes in membrane potential fluctuations and EPSP-like events, along with increased input resistance suggest that synaptic input may be reduced to RfHp neurons during seizures.

Discussion

In this study, we overcame the technical challenges of deep brain surface-to-target whole cell recordings to attain the first *in vivo* WCR of neurons in the PPT, revealing the membrane property changes in this key arousal nucleus during focal seizures. In addition to replicating prior extracellular data documenting a subset of cholinergic neurons with reduced firing during seizures [5], we found membrane potential hyperpolarization accompanied by increased input resistance, decreased spontaneous membrane potential fluctuations and reduced EPSP-like

events during seizures. These results suggest that reduced firing in putative cholinergic (RfHp) PPT neurons may arise from decreased excitatory synaptic input during seizures.

Specifically, on the presumption that changes in synaptic input to these neurons sufficient to change firing and membrane potential would produce measurable changes in input resistance, continuous measurement of input resistance during the transition from baseline to seizure activity were made. These measurements reveal an increase in the ictal R_{in} of RfHp neurons that is not seen in non-ChAT, non-RfHp neurons. In addition, subthreshold synaptic input was probed by analyzing membrane potential variance, depicted graphically through voltage histograms, and by identifying EPSP-like events morphologically. These analyses found a decrease in membrane potential variance and reduced EPSP-like events in RfHp neurons during seizures. Taken together, hyperpolarization coupled with increased R_{in}, less V_m variance and reduced EPSP-like activity is consistent with—though not specific for—a withdrawal of excitatory synaptic input underlying the reduced activity of these PPT neurons.

The reduction in firing of RfHp neurons during seizures was a robust validation of prior work illustrating the reduction in cholinergic arousal observed in focal hippocampal seizures [5]. The hyperpolarization accompanying the reduction in firing was the first clue as to the physiologic changes underlying the changes in neuronal firing. Postsynaptic hyperpolarization of a neuron could be caused by active inhibition, for example by receiving GABAergic input opening chloride channels. If the dominant input causing this hyperpolarization was increased GABAergic input, one would anticipate a decrease in R_{in} to accompany the opening of channels [28]. Another possibility for hyperpolarization to occur downstream of changes in synaptic input is for a sudden decrease in baseline excitatory synaptic input, which could lead to reduction in depolarizing current. The consistent increases in R_{in} observed accompanying the

hyperpolarization of RfHp neurons present a cogent argument against direct GABAergic input on these neurons as the dominant mechanism of their reduced activity.

Neurons *in vivo* are bombarded by synaptic activity that is integrated into that neuron's rate of firing [29, 30]. Because one explanation for the increase in R_{in} observed during seizures is a reduction in excitatory synaptic input, it follows that measures of synaptic input on RfHp neurons might show a decrease during seizures. A voltage histogram of a neuron with no synaptic input and which could perfectly maintain its physiologic V_m would appear as a single narrow impulse at the constant V_m value. The more synaptic input on this hypothetical neuron, the more its V_m would fluctuate, and the wider the histogram would spread from the mean, increasing measures of variance. Thus, V_m variance was used as one measure of synaptic input, visually depicted in V_m histograms. In agreement with our hypothesis, there was indeed a significant reduction in V_m variance during seizures, supporting the notion that a reduction in synaptic input may underlie the changes in firing activity seen in RfHp neurons during seizures.

When studying postsynaptic potentials (PSPs), excitatory postsynaptic potentials (EPSPs) or mini-EPSPs (mEPSPs), distinguishing these events in current-clamp recordings can be made clearer by the uses of voltage-gated channel blockers to reduce the contamination of data by action potentials, as well as having a known stimulus—e.g. an external input or an action potential from a nearby neuron—after which to focus data analysis [24, 31]. While we did not have these advantages, EPSP and mEPSP morphology has been described in detail and is the centerpiece of many PSP analyses of current-clamp data [24, 25, 32, 33]. Although amplitude of PSPs can vary widely based on experimental conditions like cellular distance for synaptic event from recording pipette, the impact of these conditions on rate of rise appears less pronounced. A positive deflection of $\geq$0.4mV in $\leq$2ms was chosen as criteria for EPSP-like events based on rise-

times and amplitudes of EPSPs reported in the literature [24, 25, 34]. Despite the shortcomings previously mentioned, advantages of such morphological analyses of discrete positive fluctuations V_m include protection from biases from slower changes in membrane potential, such as those associated after-hyperpolarizations of action potentials, as those contributions may be difficult to eliminate from broader analyses of membrane potential variance. The finding of decreased EPSP-like events during the ictal period of RfHp neurons provides additional evidence in favor of reduced excitatory input underlying the increased in R_{in} and concomitant reduction in both membrane potential and neuronal firing observed during seizures in RfHp neurons.

Evidence continues to build suggesting that impairments in consciousness accompanying seizures are not simply a function of acute over-activation of cortical neurons, but rather involve far-reaching effects of seizures on subcortical arousal systems [5, 8, 9, 18, 35]. Neurons of the PPT are the major source of cholinergic input to the thalamus [20, 21, 36] and have been shown to play a role in cortical transitions between slow-wave, low-arousal states to a higher arousal state [2, 4], as well as the opposite direction, from cortical fast-to-slow activity associated with acute depression in arousal in a seizure model [5]. In addition, activation through electrical or optogenetic stimulation of ascending cholinergic nuclei such as the PPT has been shown to abolish spindles and slow-waves on EEG and induce fast-activity, mirroring transitions from sleep to wake [37, 38, 39]. Building on prior work that identified PPT and forebrain cholinergic nuclei as elements of the subcortical arousal system showing evidence of functional impairment during seizures [5], the purpose of this study was to uncover synaptic mechanisms of reduced firing in cholinergic neurons in the PPT.

While this study does answer to calls for more *in vivo* WCR to contribute to understanding or relative contributions of excitation and inhibition in regulation of single neuron

electrophysiology [12], it does not do so through distinguishing excitatory from inhibitory conductance in voltage clamp. A short-coming of the model and technique developed in this study is that because seizures must be spaced out in time to avoid inducing a refractory state in the hippocampus, neurons often were lost or had increased access resistance while waiting for the hippocampus to recover to trigger a second seizure. With only a single seizure available to analyze the phenotype of a neuron, compounded by a search for comparatively sparse cholinergic neurons in a heterogenous nucleus [4] using a low-yield, time-intensive technique, emphasis was placed on current-clamp recordings for the ability to characterize the neuronal membrane properties.

Of course, when making inferences about synaptic input, a limitation of input resistance is its lack of specificity—one cannot distinguish excitatory from inhibitory currents based on R_{in} alone. However, R_{in} does become useful in the presence of other physiological data to provide clues as to the source and effect of these changes in resistance—namely changes in membrane potential and firing profiles, to which the current-clamp recordings carried out in this study offered convenient access. Moreover, direct measurements of input resistance can also give clues as to possible contributions of shunting inhibition [22, 23], which, as evidenced by the increase in R_{in}, does not appear to be the mechanism of inhibition in this case.

Using V_m histograms as a measure of synaptic input is another non-specific marker. It does not take into consideration morphology or directionality of V_m fluctuations that might give clues as to whether they are due to EPSPs or IPSPs. This shortcoming was addressed by buttressing this evidence with a morphologically-based analysis to identify positive fluctuations in membrane potential consistent with EPSPs, and conservatively referred to here as EPSP-like events. Another limitation to the present study is the sample size of RfHp neurons recorded. This

is a function of the time-intensive, low-yield experiments that follow from combining an acute *in vivo* model of limbic seizures with performing WCR deep below the brain's surface. More neurons are presumably always better, but in the presence of strong prior work with which to correlate functional neuronal characteristics and clear trends in firing activity and R_{in}, the authors believe that the present results are nevertheless of value to the field.

The question now looms as to where the baseline excitatory input that is purportedly withdrawn during seizures might originate. The PPT receives afferents from many areas, including the basal ganglia, thalamus, limbic system and cortex [19, 21, 40, 41]. Theorizing as to which of these specifically underlie the ictal withdrawal of excitatory tone would be premature. However, these findings fit with prior work suggesting that network inhibition during focal limbic seizures arises from a polysynaptic mechanism, based on the latencies observed between activation of inhibitory lateral septal regions and initiation of slow waves in the cortex [8].

In summary, putative cholinergic neurons of the PPT show a pattern of reduced firing and hyperpolarization, accompanied by increased input resistance, reduced V_m variance and reduced EPSP-like activity during seizures. These properties of RfHp neurons support a mechanism of decreased excitatory input as the basis for decreased subcortical arousal originating in PPT. These results run against prevailing conceptions of seizures as carrying out their main effects through barrages of synchronized neuronal firing and provide subcellular evidence of ictal alterations of neurophysiology through reductions in synaptic activity. This is an early step toward understanding the afferent drive of the PPT and its contribution to PPT activity [4].

As clinical advances in treatment of neurophysiologic disorders begin to rely more on neuromodulation [42, 43, 44], studies of the basic neuronal mechanisms of functional pathology become less esotericisms and closer to clinical targets for disease-modifying therapies. Deep

brain stimulation for Parkinson's disease is one example of clear translation from basic, functional neuroscience to new disease therapies[45]. Finer and more selective control over neuronal function continues to grow[46] and, as it does, the limiting factor to developing new neurophysiology-based treatments is the detailed information on how neurons are perturbed in pathologic states. Single-neuron studies such as presented in the present study will inform innovative ways to understand and address depressed arousal circuits in temporal lobe epilepsy.

References

1. Moruzzi G, Magoun HW. Brain stem reticular formation and activation of the EEG. *Electroencephalography and clinical neurophysiology* **1**, 455-473 (1949).

2. Steriade M, Datta S, Pare D, Oakson G, Dossi RC. Neuronal activities in brain-stem cholinergic nuclei related to tonic activation processes in thalamocortical systems. *Journal of Neuroscience* **10**, 2541-2559 (1990).

3. Mena-Segovia J, Sims HM, Magill PJ, Bolam JP. Cholinergic brainstem neurons modulate cortical gamma activity during slow oscillations. *The Journal of physiology* **586**, 2947-2960 (2008).

4. Mena-Segovia J, Bolam JP. Rethinking the Pedunculopontine Nucleus: From Cellular Organization to Function. *Neuron* **94**, 7-18 (2017).

5. Motelow Joshua E, *et al.* Decreased Subcortical Cholinergic Arousal in Focal Seizures. *Neuron* **85**, 561-572 (2015).

6. Mishra AM, *et al.* Where fMRI and electrophysiology agree to disagree: corticothalamic and striatal activity patterns in the WAG/Rij rat. *Journal of Neuroscience* **31**, 15053-15064 (2011).

7. Blumenfeld H. Functional MRI studies of animal models in epilepsy. *Epilepsia* **48**, 18-26 (2007).

8. Englot DJ, Modi B, Mishra AM, DeSalvo M, Hyder F, Blumenfeld H. Cortical deactivation induced by subcortical network dysfunction in limbic seizures. *The Journal of neuroscience : the official journal of the Society for Neuroscience* **29**, 13006-13018 (2009).

9. Englot DJ, Mishra AM, Mansuripur PK, Herman P, Hyder F, Blumenfeld H. Remote effects of focal hippocampal seizures on the rat neocortex. *The Journal of neuroscience : the official journal of the Society for Neuroscience* **28**, 9066-9081 (2008).

10. Zhan Q, *et al.* Impaired Serotonergic Brainstem Function during and after Seizures. *The Journal of Neuroscience* **36**, 2711 (2016).

11. Wehr M, Zador AM. Balanced inhibition underlies tuning and sharpens spike timing in auditory cortex. *Nature* **426**, 442-446 (2003).

12. Isaacson Jeffry S, Scanziani M. How Inhibition Shapes Cortical Activity. *Neuron* **72**, 231-243 (2011).

13. Higley MJ, Contreras D. Balanced excitation and inhibition determine spike timing during frequency adaptation. *The Journal of neuroscience : the official journal of the Society for Neuroscience* **26**, 448-457 (2006).

14. Neher E, Sakmann B. Single-channel currents recorded from membrane of denervated frog muscle fibres. (1976).

15. Sakmann B. Patch pipettes are more useful than initially thought: simultaneous pre- and postsynaptic recording from mammalian CNS synapses in vitro and in vivo. *Pflügers Archiv* **453**, 249-259 (2006).

16. Sugiyama D, *et al.* In vivo patch-clamp recording from locus coeruleus neurones in the rat brainstem. *The Journal of physiology* **590**, 2225-2231 (2012).

17. Martins ARO, Froemke RC. Coordinated forms of noradrenergic plasticity in the locus coeruleus and primary auditory cortex. *Nature Neuroscience* **18**, 1483-1492 (2015).

18. Blumenfeld H. Impaired consciousness in epilepsy. *The Lancet Neurology* **11**, 814-826 (2012).

19. Benarroch EE. Pedunculopontine nucleus: functional organization and clinical implications. *Neurology* **80**, 1148-1155 (2013).

20. Mesulam M, Mufson E, Wainer B, Levey A. Central cholinergic pathways in the rat: an overview based on an alternative nomenclature (Ch1–Ch6). *Neuroscience* **10**, 1185-1201 (1983).

21. Mesulam M, Geula C, Bothwell MA, Hersh LB. Human reticular formation: cholinergic neurons of the pedunculopontine and laterodorsal tegmental nuclei and some cytochemical comparisons to forebrain cholinergic neurons. *Journal of Comparative Neurology* **283**, 611-633 (1989).

22. Mitchell SJ, Silver RA. Shunting Inhibition Modulates Neuronal Gain during Synaptic Excitation. *Neuron* **38**, 433-445 (2003).

23. Holt GR, Koch C. Shunting inhibition does not have a divisive effect on firing rates. *Neural computation* **9**, 1001-1013 (1997).

24. Mason A, Nicoll A, Stratford K. Synaptic transmission between individual pyramidal neurons of the rat visual cortex in vitro. *Journal of Neuroscience* **11**, 72-84 (1991).

25. Koch C. *Biophysics of computation: information processing in single neurons*. Oxford university press (2004).

26. Kundishora AJ, *et al.* Restoring Conscious Arousal During Focal Limbic Seizures with Deep Brain Stimulation. *Cereb Cortex* **27**, 1964-1975 (2017).

27. Paladini CA, Iribe Y, Tepper JM. GABA(A) receptor stimulation blocks NMDA-induced bursting of dopaminergic neurons in vitro by decreasing input resistance. *Brain Research* **832**, 145-151 (1999).

28. Steriade M. Acetylcholine systems and rhythmic activities during the waking–sleep cycle. *Progress in brain research* **145**, 179-196 (2004).

29. Destexhe A, Paré D. Impact of network activity on the integrative properties of neocortical pyramidal neurons in vivo. *Journal of neurophysiology* **81**, 1531-1547 (1999).

30. Chance FS, Abbott L, Reyes AD. Gain modulation from background synaptic input. *Neuron* **35**, 773-782 (2002).

31. Deweese MR, Zador AM. Shared and private variability in the auditory cortex. *Journal of neurophysiology* **92**, 1840-1855 (2004).

32. Okun M, Lampl I. Instantaneous correlation of excitation and inhibition during ongoing and sensory-evoked activities. *Nat Neurosci* **11**, 535-537 (2008).

33. DeWeese MR, Zador AM. Non-Gaussian Membrane Potential Dynamics Imply Sparse, Synchronous Activity in Auditory Cortex. *The Journal of Neuroscience* **26**, 12206-12218 (2006).

34. Magee JC, Cook EP. Somatic EPSP amplitude is independent of synapse location in hippocampal pyramidal neurons. *Nature neuroscience* **3**, 895 (2000).

35. Englot DJ, Blumenfeld H. Consciousness and epilepsy: why are complex-partial seizures complex? *Progress in brain research* **177**, 147-170 (2009).

36. Williams JA, Comisarow J, Day J, Fibiger HC, Reiner PB. State-dependent release of acetylcholine in rat thalamus measured by in vivo microdialysis. *Journal of Neuroscience* **14**, 5236-5242 (1994).

37. McCormick DA, Bal T. Sleep and arousal: thalamocortical mechanisms. *Annual review of neuroscience* **20**, 185-215 (1997).

38. Steriade M, Amzica F, Nunez A. Cholinergic and noradrenergic modulation of the slow (approximately 0.3 Hz) oscillation in neocortical cells. *Journal of neurophysiology* **70**, 1385-1400 (1993).

39. Furman M, *et al.* Optogenetic stimulation of cholinergic brainstem neurons during focal limbic seizures: Effects on cortical physiology. *Epilepsia* **56**, e198-202 (2015).

40. Usunoff KG, Itzev DE, Lolov SR, Wree A. Pedunculopontine tegmental nucleus. Part I: Cytoarchitecture, transmitters, development and connections. *Biomedical Reviews* **14**, 95-120 (2003).

41. Pahapill PA, Lozano AM. The pedunculopontine nucleus and Parkinson's disease. *Brain* **123**, 1767-1783 (2000).

42. Theodore WH, Fisher RS. Brain stimulation for epilepsy. *The Lancet Neurology* **3**, 111-118 (2004).

43. Gummadavelli A, *et al.* Neurostimulation to improve level of consciousness in patients with epilepsy. *Neurosurgical focus* **38**, E10 (2015).

44. Shah SA, Schiff ND. Central thalamic deep brain stimulation for cognitive neuromodulation–a review of proposed mechanisms and investigational studies. *European Journal of Neuroscience* **32**, 1135-1144 (2010).

45. Bergman H, Wichmann T, DeLong MR. Reversal of experimental parkinsonism by lesions of the subthalamic nucleus. *Science* **249**, 1436-1438 (1990).

46. Gradinaru V, *et al.* Molecular and cellular approaches for diversifying and extending optogenetics. *Cell* **141**, 154-165 (2010).